Quantitative analysis of static yield stress variation in thickened tailings in compaction zone based on fine structure

Gezhong Chen [a,d], Cuiping Li [a,d,e*], Zhuen Ruan [a,b,d,e*], Raimund Bürger [c], Bingheng Yan[a,d], Chen Hu [a,d] , Xue Li [a,d]

a. *Key Laboratory of the Ministry of Education of China for High-efficient Mining and Safety of Metal Mines, University of Science and Technology Beijing, Beijing 100083, PR China*

b. *Shunde Graduate School, University of Science and Technology Beijing, Foshan 528399, PR China*

c. *CI2MA and Departamento de Ingeniería Matemática, Facultad de Ciencias Físicas y Matemáticas, Universidad de Concepción, Casilla 160-C, Concepción, Chile*

d. *School of Civil and Resource Engineering, University of Science and Technology Beijing, Beijing 100083, PR China*

e. *Key Laboratory of Safe and Green Mining of Metal Mines with Cemented Paste Backfill, National Mine Safety Administration, University of Science and Technology Beijing, Beijing 100083, PR China*

*Corresponding authors: E-mail: cpli@ustb.edu.cn (C Li), E-mail: ustb_ruanzhuen@hotmail.com (Z Ruan).

Abstract

In the tailings thickening process, the poor flowability of the high-concentration tailings slurry is likely to cause slurry hardening at the bottom of the vertical sand silo and rake blockage of the thickening machine, which will hurt the safe production of the mine and pollutes the environment. Therefore, the effect of slurry concentration on the static yield stress of the slurry with and without shear conditions was investigated using the full tailings of iron ore as raw material in this study. A comparative analysis of the static yield stress of thickened tailings and fresh mixing slurry with the same concentration and particle gradation was completed. The fine structural parameters of the thickening bed with and without shear were obtained by computed tomography. The effects of the structural parameters of the drainage channels in the thickening bed and the changes in the content of coarse particles with diameters ranging from 45-300 μm on the porosity of the thickening bed were analyzed. The effect of the fluctuation of the thickening bed's porosity on the slurry's static yield stress was also investigated. The results show that the thickened tailings is non-homogeneous. The concentration of the slurry, the number and volume of coarse particles with diameters in the range of 75-300 μm increases with decreasing bed height. Analysis of the pore-network model based on the structural equivalents of the drainage channels revealed that the pore volumes with equivalent diameters in the range of 50-250 μm are the largest and are the main storage space for water in the bed. Compared with the spherical pore structure, the stick throat channel structure is the main component of the drainage channel structure in the bed. The slurry rheology measurements show that the static yield stress of the thickened tailings is 5.3-61.3 times higher than the static yield stress of the fresh mixing slurry for the same slurry concentration and particle gradation. Our analyses revealed that the fluctuation of the porosity of the slurry also has an essential effect on the static yield stress of the thickened tailings. For the first time, we propose to use the coefficient of variation in bed porosity to quantify the difference in static yield stress values between thickened tailings and fresh mixing slurry and draw the necessary conclusion that the static yield stress of slurry decreases with the reduction of the coefficient of variation in bed porosity under the same conditions of slurry concentration and particle gradation. Based on the results of our research, it was applied in an iron ore mine in China, where vertical sand silo was used as the thickening equipment to solve the problem of slurry hardening in the silo and to achieve safe and efficient filling production.

Keywords: tailings thickening; static yield stress; particle gradation; pore-network model

1 Introduction

During mining, a large amount of low-concentration tailings slurry will be produced. If not handled correctly, it will bring severe natural disasters (Glotov et al., 2018; Rico et al., 2008). Mines are used to dispose of low-concentration tailings slurry by discharging it directly into tailings ponds. However, dam failure of tailings ponds and discharge of tailings wastewater have caused severe environmental damage, deaths, and extensive property damage (Adiansyah et al., 2015; Rana et al., 2022). Therefore, how to reasonably, effectively, and safely dispose of low-concentration tailing slurry has been a critical concern of global mining enterprises (Gao et al., 2023; Lèbre et al., 2017; Wu et al., 2022). Tailings thickening is the tailings slurry through the flocculation, bed gravity compression, and rake shear to achieve a low-concentration of tailings slurry to a high-concentration of tailings slurry transformation of technology (Ghandashtani et al., 2022; Chen et al., 2023a; Qi and Fourie, 2019; Wu et al., 2020). It provides high-concentration underflow for high-concentration slurry storage and paste backfill in mines, reduces the water consumption of the mining industry, saves the economic cost of filling, and has been widely used in mines (Mashifana and Sithole, 2021; Qi and Fourie, 2019; Trampus and França, 2020; Wu et al., 2022; Yin et al., 2020).

Vertical sand silo and thickener, as commonly used equipment in the thickening of mine tailings, have the advantages of simple operation, large processing capacity, and low operating costs (Arjmand et al., 2019; Langlois and Cipriano, 2019). Scholars have carried out a lot of research on the flocculation effect, floc settling behavior and underflow concentration improvement of tailings in a vertical sand silo and thickeners and achieved remarkable results. Regarding the flocculation effect of tailings, scholars have researched the optimization of flocculation conditions and studied the effects of tailings slurry concentration, flocculant solution concentration, and flocculant dosage on supernatant turbidity and floc structure (Chen et al., 2023b; Wu et al., 2020). The effects of temperature and pH of the slurry on the flocculation effect were also investigated (O'Shea et al., 2010; Peng et al., 2023; Zhu et al., 2023). Scholars also explored the impact of flocculant type, flocculant molecular weight, and ionic degree on flocculation effect from the chemistry perspective, and they analyzed the impact of tailings element on floc structure (Leite and Reis, 2020; Lin et al., 2023; Peng et al., 2023; Sabah and Erkan, 2006; Walch et al., 2022). Some other scholars have analyzed the effect of fluid shear on flocculation, showing that the floc structure is more prone to break with high shear stress (Carissimi and Rubio, 2015; Wang et al., 2020; Yu et al., 2011).

Regarding floc settling behavior, scholars have analyzed the change in the equivalent diameter of flocs and the floc breakage mechanism during the settling process (Chen et al., 2023b; Ye et al., 2023). The effect of floc structure breakage on the fractal dimension of flocs during settling is also investigated (Asensi and Alemany, 2022; Liu et al., 2021). Relevant scholars have analyzed the changing rules of the breakage factor and strength factor of flocs during the settling process (He et al., 2023; Murujew et al., 2020). The interaction mechanism between the fluid flow field and floc

transport during the settling process was obtained (Fawell et al., 2021; He et al., 2023). Some scholars have also studied the changes in physical properties during floc settling under different flocculation conditions and optimized the flocculation conditions based on the changes in floc density and settling velocity (Chen et al., 2023b; Ye et al., 2023).

In terms of the increase of underflow concentration, scholars have studied the effect of tailings bed height and slurry residence time on the increase of underflow concentration and also compared the effect of shear conditions on underflow concentration (Li et al., 2023a; Zhu et al., 2020). The results showed that the concentration of the underflow slurry was higher with shear than without shear (Huazhe et al., 2020; Li et al., 2023a). Some scholars have analyzed the mechanism of bottom flow concentration enhancement from the aspect of microstructure, showing that under bed pressure and rake shear, the large drainage channel structure in the bed ruptures into small drainage channels, resulting in the reduction of drainage channel volume and the increase of slurry concentration (Chen et al., 2023a; Chen et al., 2024; Jiao et al., 2021). Some scholars have also analyzed the change in permeability of thickened tailings with slurry concentration, showing that the permeability of thickened tailings decreases with increasing slurry concentration, i.e., it is difficult to increase the concentration of high-concentration slurry again (Chen et al., 2024).

Scholars have researched the flocculation effect, settlement behavior, and underflow concentration increase of the tailings thickening through the above research. However, there are few studies on the rheology of slurry in the thickening equipment. The poor flowability of the high-concentration slurry will cause the hardening of the slurry in the vertical sand silo and the rake blockage of the thickener, which will adversely affect the smooth discharge of the thickening underflow slurry (Jia et al., 2020; Tan et al., 2017; Zhu et al., 2023). Therefore, there is an urgent need to conduct rheological measurement experiments on the slurry in the tailings thickening process to investigate the variation in the slurry's static yield stress with the slurry's concentration. In the previous rheological measurement experiments, such as the tailings mixing and pipeline transport processes, the fresh mixing slurry was used for the measurement (Chen et al., 2023; Li et al., 2023b, 2022; Wang et al., 2021). This is not the same as the structural state of the slurry inside the vertical sand silo and thickener in the tailings thickening process. Therefore, another objective of this study is to give the correct measurement of the rheological parameters of the slurry inside the vertical sand silo and thickener in the tailings thickening process.

Inspired by the above research, two approaches are used in this study to investigate the variation rule of static yield stress of slurry with slurry concentration. The first way is to take in-situ samples of the thickening bed of tailings formed by flocculation and settling with or without shear in the thickener model. Then, rheological measurements will be carried out to obtain the slurry static yield stress change with a slurry concentration in the thickening bed. The second way is to reconfigure the fresh mixing slurry for rheological measurements based on the slurry concentration and particle gradation obtained during the measurements. On this basis, the micro-structural parameters of the drainage channel and coarse particles in the thickening bed at different heights

were obtained by computer tomography (CT). The effects of coarse particle content, volume, and structural parameters of the drainage channel on the concentration of the thickening bed were analyzed. The difference between the static yield stress of the thickening bed layer slurry and the fresh mixing slurry was also explained from the perspective of slurry porosity fluctuation. The variation law of T_{SYS} (the ratio of the static yield stress of thickened tailings to the static yield stress of fresh mixing slurry) with the variation in coefficient (CV) of porosity of thickening bed was obtained under the same concentration and particle gradation. This study is expected to provide a reliable measurement for obtaining the rheological parameters of the thickened tailings in the tailings thickening. The change rule of the static yield stress of the slurry with the concentration of the slurry was obtained. The relationship between the coefficient of variation in the thickened tailings porosity and the slurry's static yield stress was obtained, which is of practical significance for the safe operation of the mine thickening equipment.

2 Materials and Methods

This study consists of three experiments: flocculation and settling experiment (I), slurry rheology measurement experiment (II), and CT scanning experiment of the bed in the compaction zone (III). The experimental flow is shown in Fig. 1.

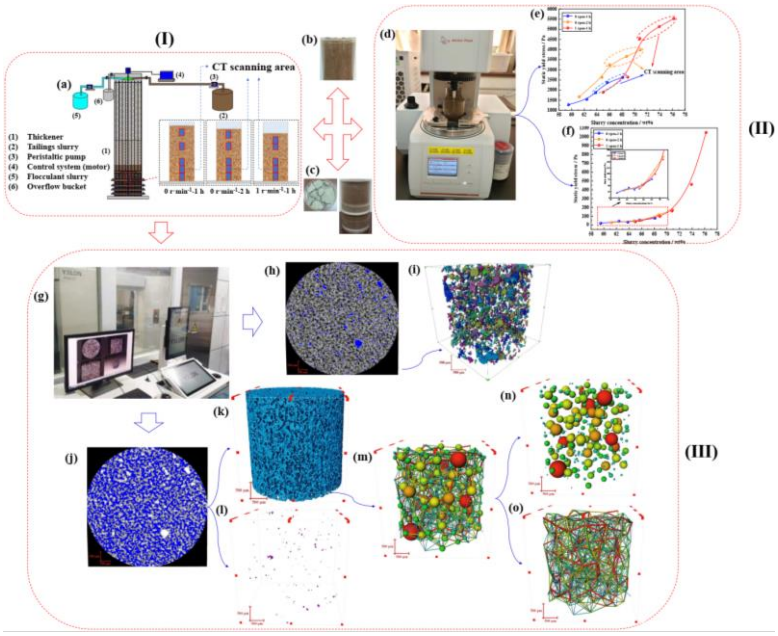

Fig. 1. Experimental flowchart: (a) flocculation and settling experiments, (b) in-situ sampling of the thickening bed, (c) fresh mixing slurry, (d) slurry rheology measurements, (e) static yield stress of the thickened tailings, (f) static yield stress of the fresh mixing slurry, (g) CT scanning experiments of the thickening bed, (h) threshold segmentation of the coarse particles, (i) 3D reconstruction of the coarse particles, (j) threshold of the drainage channel structure segmentation, (k) 3D reconstruction of connected drainage channel structures, (l) 3D reconstruction of isolated pore structures, (m) pore-network modeling of drainage channel structures, (n) spherical pore structures, (o) stick throat channel structures.

2.1 Experimental materials

The materials used in this study consisted mainly of tailings, mixing water, and flocculants.

2.1.1 Tailings

The full tailings used in this experiment were from an iron ore mine in China, and the particle size distribution (PSD) of the tailings is shown in Fig. 2 (a) (Chen et al., 2023a). We can see that the content of fine particles (-20 μm) in the tailings is more than 60wt%, and the average particle size is 22.9 μm. The specific gravity of the full tailings is 2.749 g / cm^3, and the chemical elements and their contents in the full tailings are shown in Fig. 2 (b) and Table 1, respectively (Chen et al., 2023a).

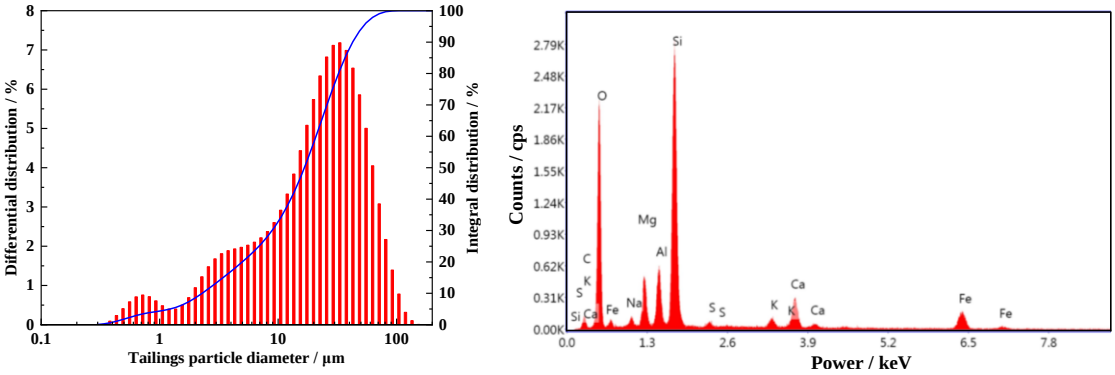

(a) (b)

Fig. 2. Physical properties of full tailings: (a) particle size distribution of tailings, (b) tailings energy spectrum.

Table 1 Chemical element analysis of tailings.

Element	C	O	Na	Mg	Al	Si	S	K	Ca	Fe
Content (%)	7.85	47.32	1.35	4.41	4.77	21.63	0.37	1.11	4.44	6.75

2.1.2 Flocculant

In the thickening process of the mine, flocculants are often used to flocculate the tailings slurry, which effectively improves the settling speed of the tailings particle and reduces the turbidity of the supernatant. There are many types of flocculant. In this experiment, the type of flocculant we used is anionic polyacrylamide, and the molecular weight is 13 million. The flocculant solution was stirred and stood for 24 hours the day before the experiment (Chen et al., 2023b).

2.2 Experimental procedures

2.2.1 Flocculation and settling experiments

We used a self-made thickener to conduct flocculation settling experiments (I) on three experimental variable conditions. Based on the preliminary experiment, the material parameters used in this experiment were determined as follows: the mass of dry tailings was 10 kg, the concentration of tailings slurry was 25wt%, the concentration of flocculant solution was 0.005wt %, and the dosage of flocculant was 30 g / t (Chen et al., 2023a).

The three experimental variable conditions are: the residence time of the slurry is 1 hour without shear (0 rpm-1 h), the residence time of the slurry is 2 hours without shear (0 rpm-2 h), and the residence time of the slurry is 1 hour with shear (1 rpm-1 h). During the experiment, the tailings slurry and flocculant solution were rapidly pumped to the thickener by a peristaltic pump. In particular, the tailings slurry was stirred at high speed using a mixer to avoid uneven distribution of tailings particles in the slurry.

2.2.2 Rheological experiment of slurry in compaction zone

The slurry rheology measurement experiment (II) is based on the experiment (I). In this experiment, we used two measurement methods to test the static yield stress of the slurry in the compaction zone. The first way is to take in-situ sampling measurements of the thickened tailings in the thickener, with 5 points sampled at different heights under each experimental condition, the sampling heights under the three experimental conditions are shown in Table 2. Slurry concentration and particle size content in the rheological measurement part were obtained. The second way is to reconfigure the fresh mixing slurry for measurement based on the particle gradation data and slurry concentration obtained in the first measurement method. Moreover, the dosage of the flocculant added is consistent with the dosage during the flocculation and settling experiments. A small mixer with 1300 rpm / min was used for 5 minutes to ensure that the tailings particles were well mixed with the mixing water and flocculant solution.

Table 2 Sampling height of rheological experimental samples

	Height / cm				
0 rpm-1 h	0-4	4-8	8-12	15-19	23-27
0 rpm-2 h	0-4	4-8	8-12	15-19	20-24
1 rpm-1 h	0-4	4-8	8-12	15-19	18-22

An Anton Paar MCR 702e rheometer measured the static yield stress of the slurry. The measured rotor is a four-leaf slurry rotor, model ST20-4V-40 / 116; the rotor diameter is 20 mm, and the height is 40 mm. The inner diameter of the measuring vessel is 50 mm, and the height is 100 mm. According to the exploration of the pre-experiment, the static yield measurement of the slurry in this experiment adopts constant shear, the shear rate is 0.3 s^{-1}, the interval time of data sampling is 1 s, and the measurement time is 90 s.

2.2.3 CT scanning experiment of slurry in compaction zone

The CT scanning experiment (III) of the slurry in the compaction zone was carried out based on experiment (II) and experiment (I). We carried out an in-situ sampling of the slurry in the compaction area of the flocculation settling experiment and carried out CT scanning experiments. According to the preliminary experiment, the outer diameter of the sampling tube in this CT scanning experiment was 21.0 mm, and the height was 40 mm. In addition, to reduce the damage of the tube wall friction on the bed fine structure data and to avoid the disturbance of the bed fine

structure data during the sampling process, we only analyze the data for the tailings bed with the sampling tube center diameter and height of 13.6 mm and 32.0 mm, respectively. Combined with the rheological measurement results of the experiment (II), we sampled 3 points at different heights of the slurry under each experimental condition, and a total of 9 points were sampled under three experimental conditions for CT scanning. It should be noted that the CT scanning area of the thickened tailings must be consistent with the measurement part of the four-leaf slurry rotor during the rheological measurement process. The sampling heights under the three experimental conditions are shown in Table 3.

Table 3 Sampling height of CT experimental samples

	Height / cm		
0 rpm-1 h	0-4	4-8	8-12
0 rpm-2 h	0-4	4-8	8-12
1 rpm-1 h	0-4	4-8	8-12

The instrument used for this CT scanning experiment was a high-resolution CT instrument (FF35, YXLON, Germany). According to the previous experiments, the best scanning effect can be achieved when the scanning voltage is 100 KV, and the scanning current is 200 μA (G. Chen et al., 2023a). The resolution of the scanned voxels of this sample is 12.9 μm, and the pixels of each image are 2146*2146.

3 Results

3.1 Slurry concentration and particle distribution in the compaction zone

As shown in Fig. 3, the slurry concentration gradually increases with decreasing bed height with and without shear (Chen et al., 2023a). Moreover, the slurry concentration with a bed residence time of 2 h is higher than that with a bed residence time of 1 h without shear (Li et al., 2023a). We compared the slurry concentration in the bed with and without shear and found that the slurry concentration in the bed was higher than without shear (Jiao et al., 2021; Li et al., 2023a). In addition, the thickened tailings in the rheological measurement zone was wet-screened by a vibrating sieve machine and classified into 5 parts according to the tailing particle size: <38 μm, 38-45 μm, 45-75 μm, 75-150 μm, and 150-300 μm (Qi et al., 2018). Table 3 records the mass percentage of each particle size range in the thickened tailings in the rheological measurement area. It can be seen that with the decrease of bed height, the content of particle size in the range of < 38 μm, 38-45 μm, and 45-75 μm in the slurry decreases gradually, and the content of particle size in the range of 75-150 μm and 150-300 μm increases gradually.

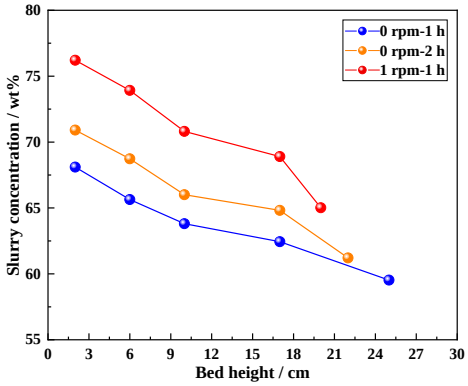

Fig. 3. Variation in slurry concentration with bed height

Table 3 Variation in slurry particle content in the compaction zone

Content / wt%		<37 μm	37-45 μm	45-75 μm	75-150 μm	150-300 μm
	23-27 cm	47.8	6.8	18.7	13.6	13.1
	15-19 cm	45.5	5.6	18.6	15.4	14.9
0 rpm-1 h	8-12 cm	41.9	4.9	17.3	17.4	18.5
	4-8 cm	41.2	4.8	16.7	17.7	19.6
	0-4 cm	40.8	4.6	15.8	19.5	19.3
	20-24 cm	45.7	5.1	18.3	17.4	13.5
	15-19 cm	42.5	4.8	17.2	20.3	15.2
0 rpm-2 h	8-12 cm	38.1	4.1	15.6	21.7	20.5
	4-8 cm	37.5	3.9	16.4	20.3	21.9
	0-4 cm	37.3	3.6	15.4	21.2	22.5
	18-22 cm	48.8	7.3	21.4	15.9	6.6
	15-19 cm	41.1	5.6	19.5	18.4	15.4
1 rpm-1 h	8-12 cm	34.4	3.4	15.5	22.4	24.3
	4-8 cm	33.1	3.2	15.3	22.6	25.8
	0-4 cm	32.7	2.7	14.7	23.5	26.4

3.2 Structural parameters of coarse particles in the compaction zone

This section imported 2D greyscale images from CT scans into 3D reconstruction software (Avizo 3D, ThermoFisher, USA). Based on the threshold segmentation theory, we obtained the basic information about the tailings particles in the bed, and the relevant details are referred to in our previous research (Li et al., 2023a). To avoid identifying the fine particles gathered in the bed as large particles, we only analyzed the volume, equivalent diameter, and number of coarse tailings particles with an equivalent diameter of more than 45 μm in this study. The 3D reconstruction results of coarse particles above 45 μm in the thickening bed are shown in Fig. 4.

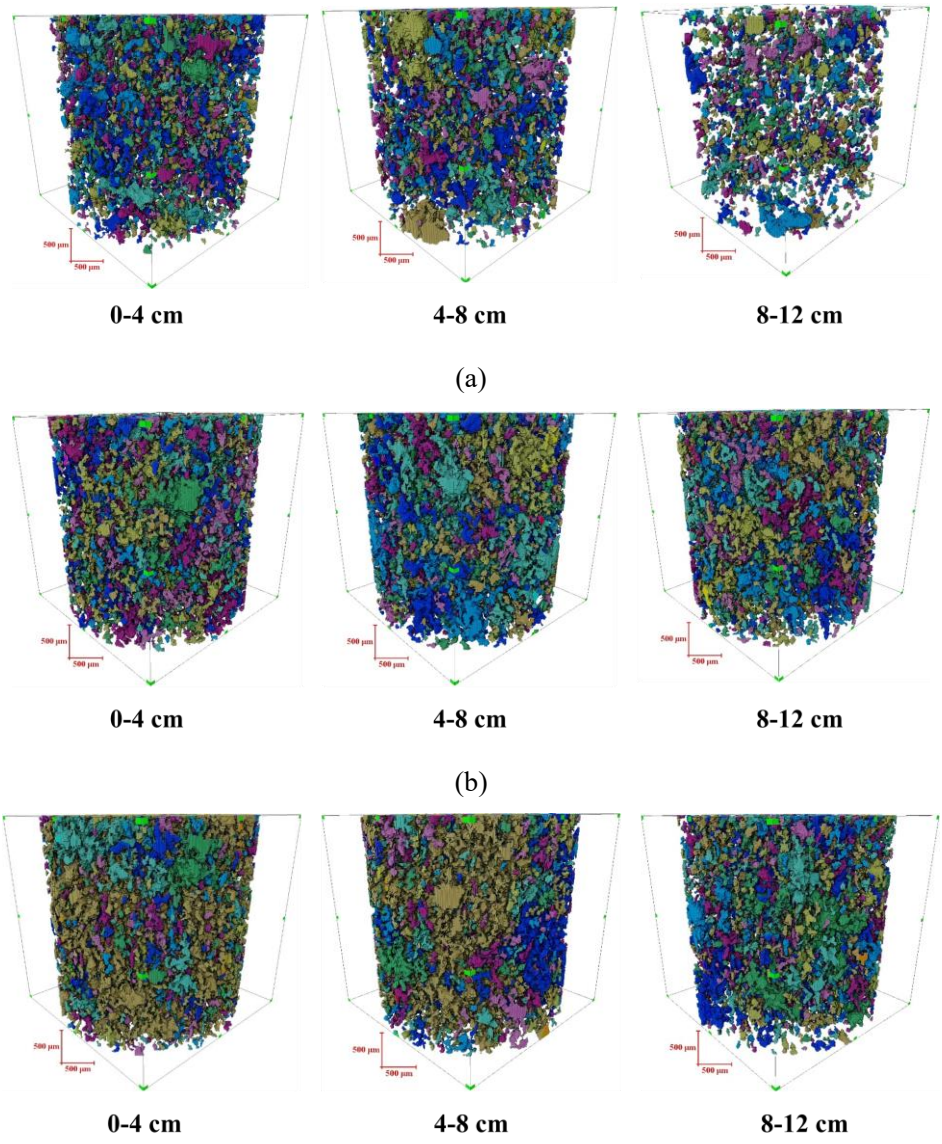

Fig. 4. 3D reconstruction of coarse particles in the bed: (a) 0 rpm-1 h, (b) 0 rpm-2 h, (c) 1 rpm-1 h.

The equivalent particle size distribution data of coarse tailings particles above 45 μm in the bed are shown in Fig. 5. As we can see, the equivalent particle size distribution of coarse particles at different bed heights is very close with or without shear. The results show that the number of coarse particles in the range of 45-75 μm is the highest, the number of coarse particles in the range of 75-150 μm is the second, and the number of coarse particles in the range of 150-300 μm is the lowest (Chen et al., 2023a).

We found that without shear conditions, the proportion of coarse particles in the range of 75-150 μm and 150-300 μm in the bed increased slightly, and the proportion of coarse particles in the range of 45-75 μm decreased slightly as the bed height decreased. At the same height, the proportion of coarse particles in the range of 75-150 μm and 150-300 μm in the bed with a slurry residence time of 2 h is higher than that with a slurry residence time of 1 h, and the proportion of coarse particles in the range of 45-75 μm is lower than that with a slurry residence time of 1 h. And

we also found that when the rake shear speed is 1 rpm, the proportion of coarse particles in the range of 75-150 μm and 150-300 μm in the bed is slightly higher than that without shear, and the proportion of coarse particles in the range of 45-75 μm is slightly lower than that without shear.

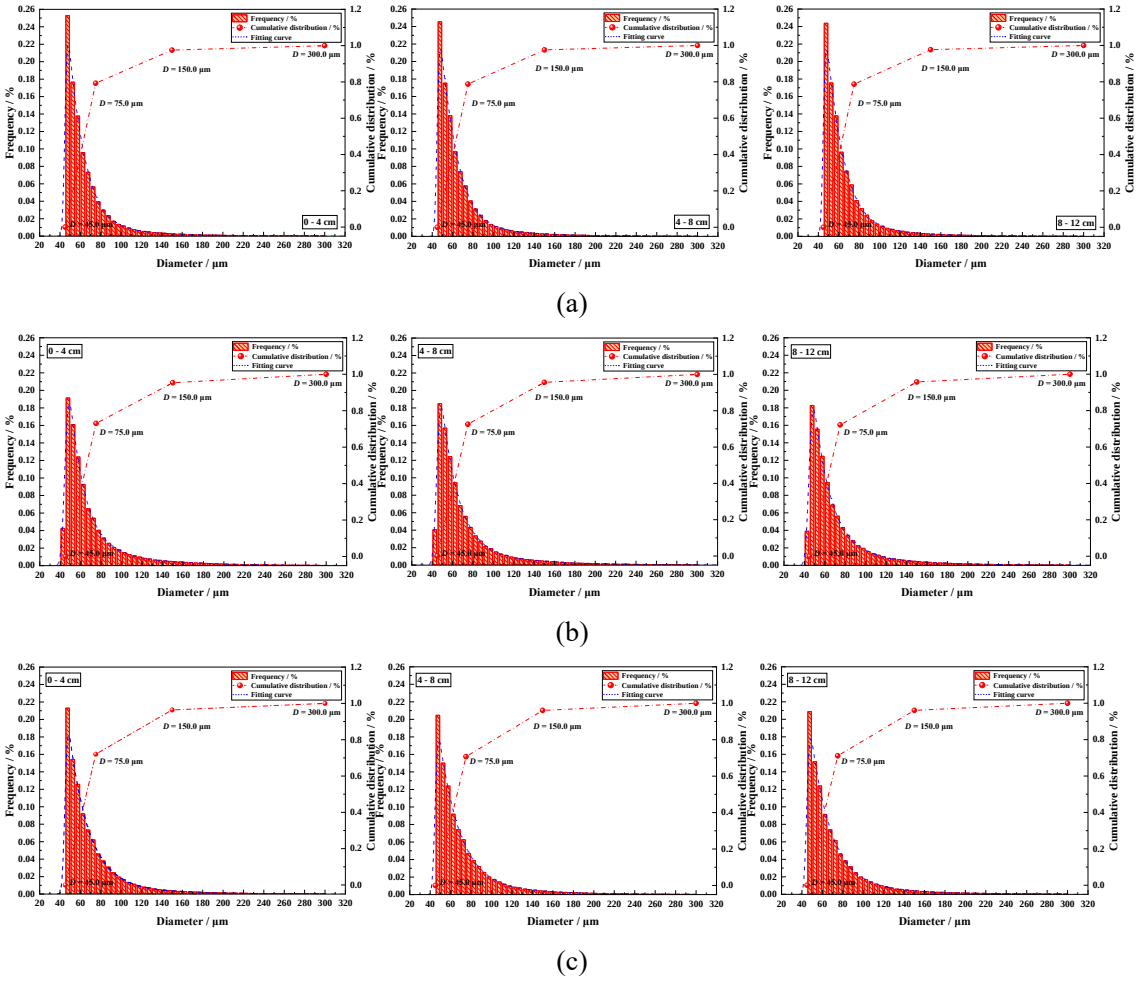

Fig. 5. Distribution of coarse particle content with particle size: (a) 0 rpm-1 h, (b) 0 rpm-2 h, (c) 1 rpm-1 h.

3.3 Structural parameters of drainage channels in the compaction zone

We also obtained 3D structures of connected and isolated drainage channels in the thickening bed based on threshold segmentation and 3D body reconstruction. Please refer to our previous research for a detailed discussion of this section (Chen et al., 2023a; Li et al., 2023a). Based on the equivalent pore-network model (PNM), we obtained the equivalent pore-and-stick of the connected drainage channel structure at different bed heights for each of the three experimental conditions, as shown in Fig. 6. Where the spherical structure represents the pore space and the stick structure represents the throat channel (Chen et al., 2023a; Jiao et al., 2021; Xiong et al., 2016).

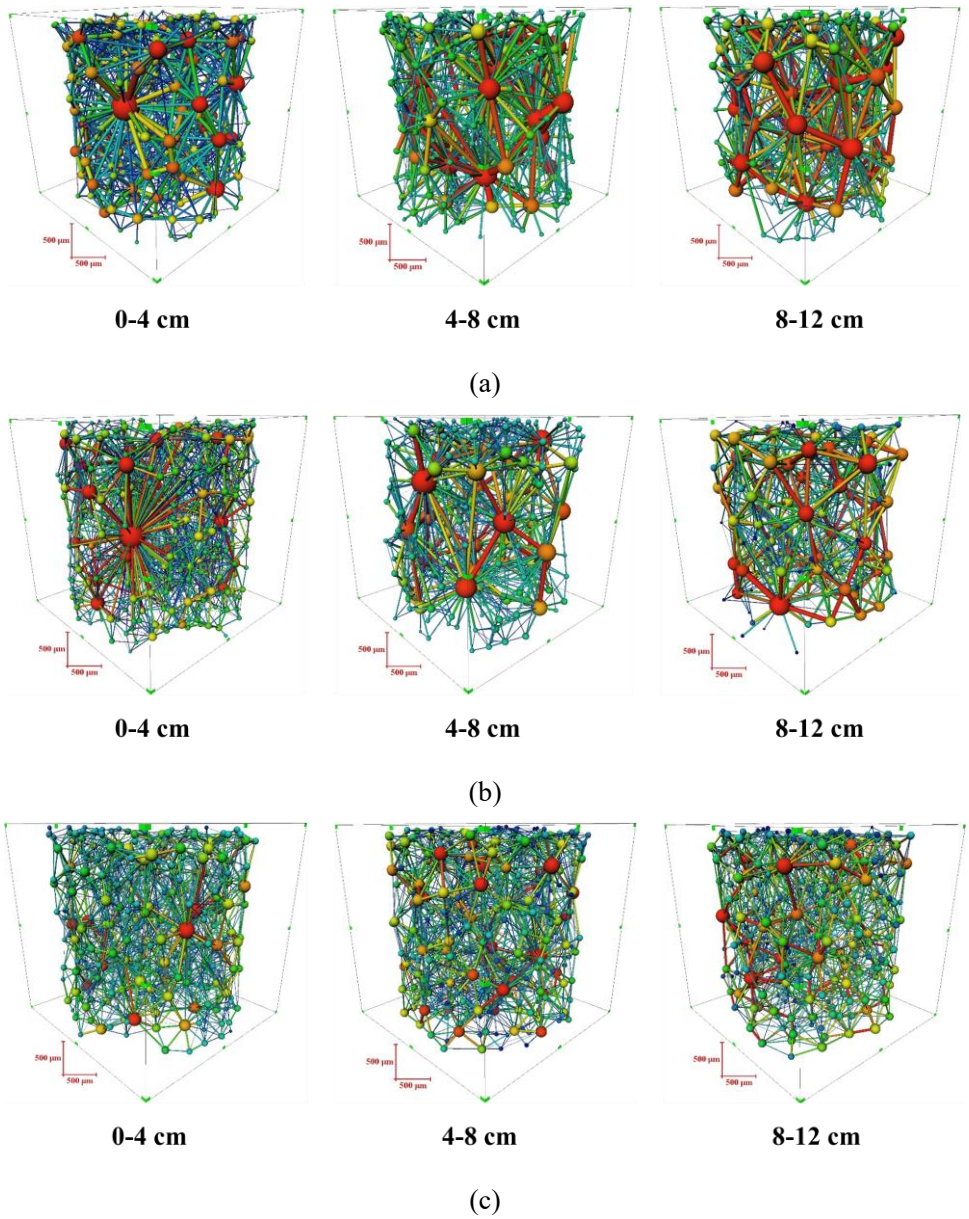

Fig. 6. PNM of the drainage channels in the thickening bed: (a) 0 rpm-1 h, (b) 0 rpm-2 h, (c) 1 rpm-1 h.

Based on the pore threshold segmentation theory and PNM (Fatt, 1956; Otus, 1979), we plotted the equivalent diameter distributions of isolated pores, spherical pores, and stick throat in the bed with bed height, respectively, as shown in Fig. 7. From Fig. 7 (a)- Fig. 7 (c), it can be seen that the equivalent diameters of the isolated pores in the bed are distributed in the range of 2.5-50 μm. The number of isolated pores in the bed increases with the decrease in bed height (Chen et al., 2023a; Jiao et al., 2021). Among them, the number of isolated pores with equivalent diameters in the 7.5-12.5 μm range was the highest. We compared the isolated pore parameters with and without shear conditions and found that the number and equivalent diameter of isolated pores increase to varying degrees with shear conditions.

The results of Fig. 7 (d)- Fig. 7 (f) and Fig. 7 (g)- Fig. 7 (i) show that the diameter of spherical pores is distributed in the range of 50-500 μm, and the diameter of stick throats is distributed in the range of 25-350 μm. As the bed height decreases, the distribution range of spherical pores and stick

throat diameters gradually decreases (Chen et al., 2024; Chen et al., 2023a; Jiao et al., 2021). The number of pores in the range of 162.5-500 μm diameter and the number of throat channels in the 157.5-350 μm diameter show a decreasing trend. The number of pores in the 50-162.5 μm diameter range and the number of throat channels in the 25-157.5 μm diameter gradually increased. The data indicate that as the bed height decreases, the large spherical pores and large throat channels in the drainage channel structure gradually change to tiny spherical pores and tiny throat channels (Chen et al., 2024; Jiao et al., 2021).

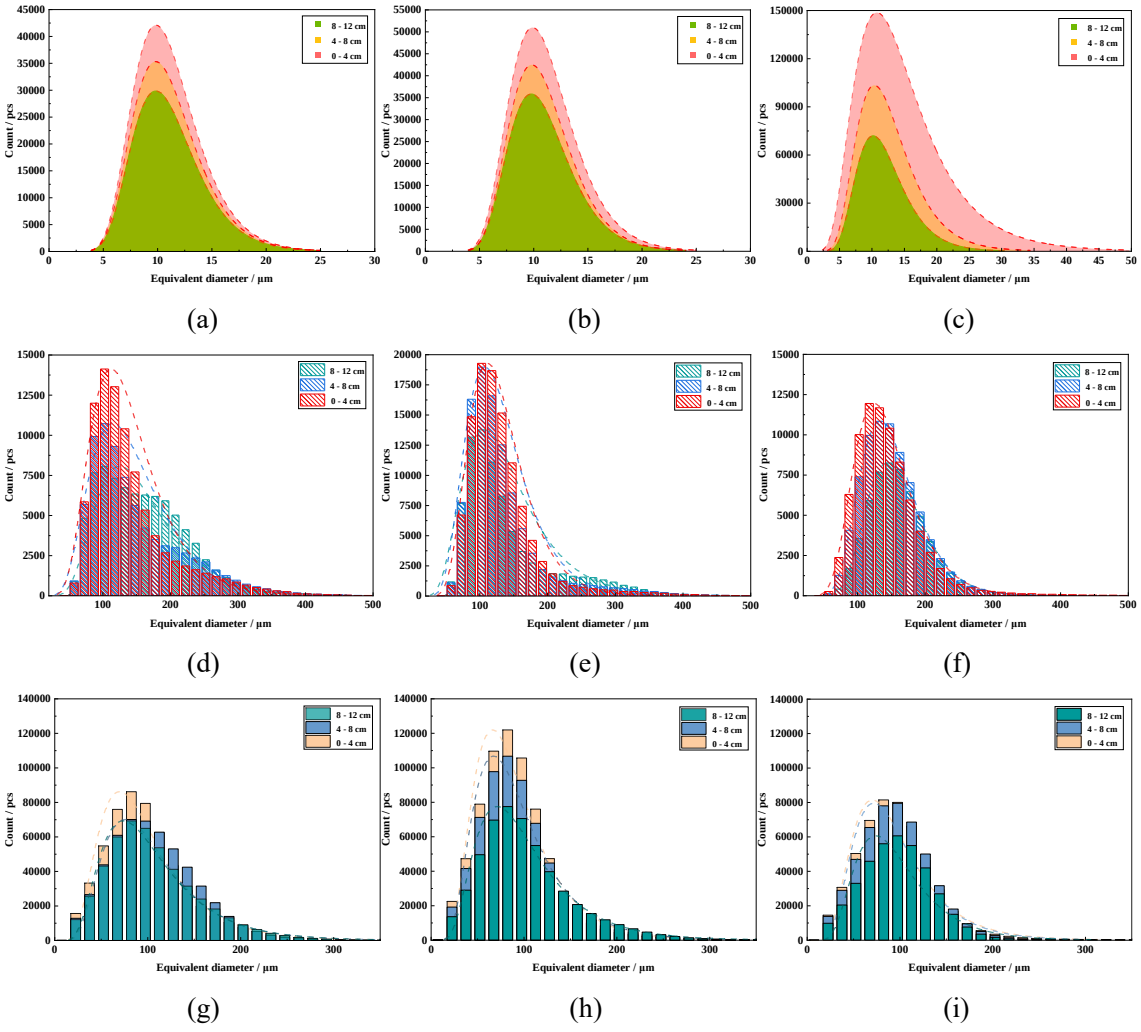

Fig. 7. Structural parameters of drainage channels in the bed: Equivalent diameter of isolated pores (a) 0 rpm-1 h, (b) 0 rpm-2 h, (c) 1 rpm-1 h. Equivalent diameter of spherical pores (d) 0 rpm-1 h, (e) 0 rpm-2 h, (f) 1 rpm-1 h. Equivalent diameter of throat channel (g) 0 rpm-1 h, (h) 0 rpm-2 h, (i) 1 rpm-1 h.

3.4 Static yield stress measurement of slurry in the compaction zone

The rheological measurement curves of the thickened tailings in the compaction zone with and without shear are shown in Fig. 8 (a)- Fig. 8 (c). The data show that the rheological curves of the thickened tailings in the compaction zone with and without shear show the same trend. The shear stress of the slurry shows a trend of increasing and then decreasing with the increase of measurement time. The shear stress of the slurry also increases with the decrease of bed height at the same shear

moment. Based on the data of slurry concentration and particle size in the rheological measurement area, we obtained the rheological measurement curves of fresh mixing slurry, as shown in Fig. 8 (d)-Fig. 8 (f). We can find that at the same shear moment, the shear stress of the slurry increases with the increase of slurry concentration, which is consistent with the findings of previous research (Li et al., 2023b; Ruan et al., 2021; Zhu et al., 2023). We compared the rheological curve of the thickened tailings in the compaction area with the rheological curve of the fresh mixing slurry and found that the two have significant differences. For the discussion of this part, we will make a detailed analysis in Section 4.

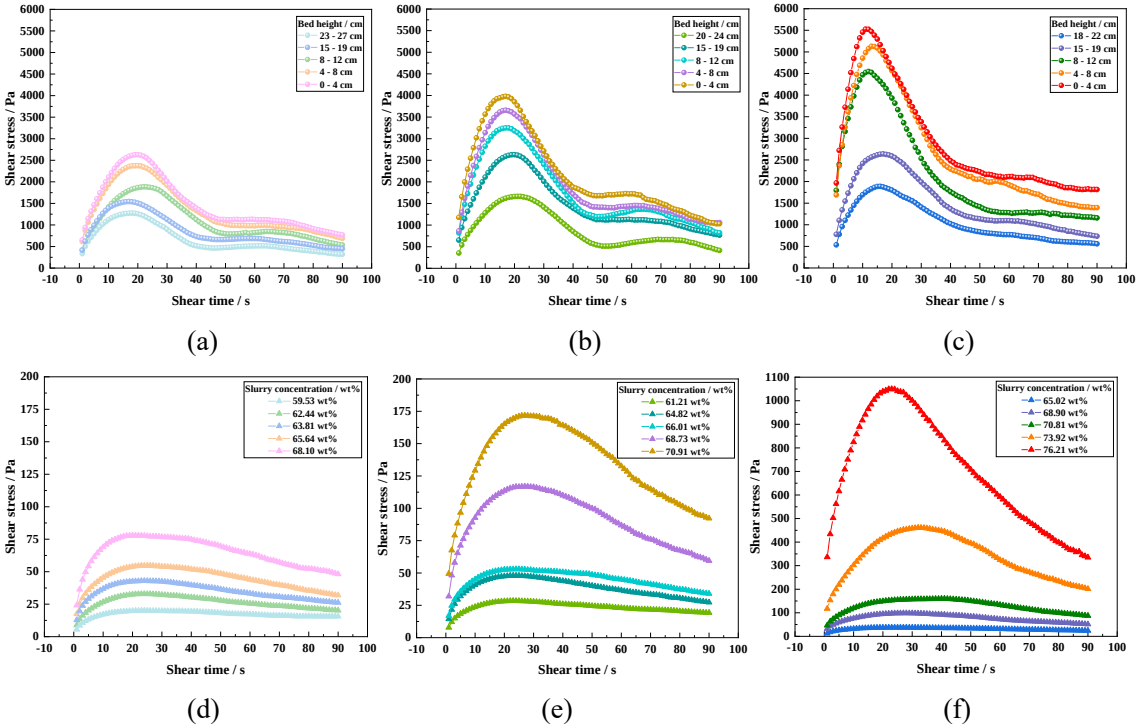

Fig. 8. Rheological measurement curves of thickened tailings: (a) 0 rpm-1 h，(b) 0 rpm-2 h，(c) 1 rpm-1 h; Rheological measurement curves of fresh mixing slurry: (d) 0 rpm-1 h，(e) 0 rpm-2 h，(f) 1 rpm-1 h.

4 Discussions

4.1 Effect of variation in coarse particle content on bed porosity

It can be seen from Fig. 9 that as the bed height decreases, the number and volume of coarse particles with a diameter of more than 45 μm in the bed increase to varying degrees. We found that there are two reasons for this result. On the one hand, in the early stage of the tailings bed structure formation, the structural strength of the tailings bed is less than the particle gravity. The coarse particles have apparent settlement behavior under gravity and accumulate at the bottom of the tailings bed (Adiguzel and Bascetin, 2019; Li et al., 2023b). On the other hand, the settlement behavior of the tailings bed structure occurs under pressure, and the height of the bed interface decreases with the increase of the residence time of the slurry, increasing the content of coarse particles per unit volume (Zhang et al., 2022). Furthermore, the settlement behavior of the bed structure is slow. When the structural strength of the slurry and the pressure of the upper bed reach

an equilibrium state, the settlement behavior of the bed no longer occurs (MacIver and Pawlik, 2022). Therefore, at the same bed height, the number and volume of coarse particles in the bed with a slurry residence time of 2 h are greater than those with a slurry residence time of 1 h (Li et al., 2023a). It is worth noting that compared with the number and volume of coarse particles in the bed without shear, the number and volume of coarse particles in the bed with shear have significantly improved. The result is mainly attributed to the shearing effect of the rake significantly increasing the bed's slurry concentration and the content of coarse particles in the unit volume (Li et al., 2023a).

In tailings thickening, the structural strength of the initially formed thickening bed is weak (MacIver and Pawlik, 2022). Under the pressure of the upper bed, the drainage channel structure is broken, reducing the equivalent diameter of the drainage channel and the volume of the drainage channel structure (Chen et al., 2024). Therefore, the porosity of the slurry decreases with the decrease in the bed height with and without shear. Before the bed structure strength and the upper bed pressure reach equilibrium, the bed structure is in a slow settlement state with the increase of slurry residence time, which promotes water discharge in the bed and further reduces the volume of the drainage channel structure. Therefore, at the same bed height, the porosity of the thickened tailings with a slurry residence time of 2 h is lower than that of the thickened tailings with a slurry residence time of 1 h (Chen et al., 2023a). During the low-speed shearing process of the rake, the rake and the water guide rod structure change the azimuthal angle of the coarse particles in the bed and form a squeezing effect on the drainage channel structure. The higher the content of coarse particles in the bed, the more pronounced the squeezing effect of coarse particles on the drainage channel structure during the rake shearing process. And the more pronounced volume reduction of the drainage channel structure, resulting in a lower bed porosity under the rake shearing condition (Li et al., 2023a).

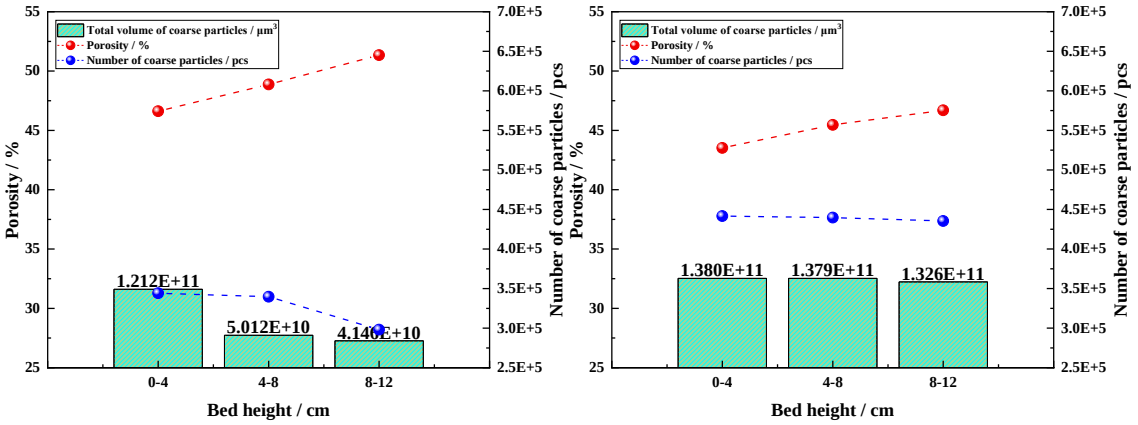

(a) (b)

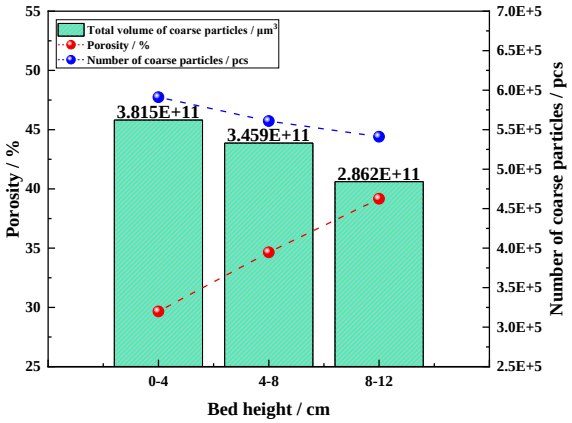

(c)

Fig. 9. Variation in bed porosity and coarse particle parameters with bed height: (a) 0 rpm-1 h, (b) 0 rpm-2 h, (c) 1 rpm-1 h.

4.2 Variation in drainage channel structural parameters with bed height

To clarify the influence of pore structure changes in different sizes in the bed on the slurry concentration, we transformed the isolated pore structure in the bed, the spherical pore structure, and the stick throat channel structure in the PNM into the same spherical pore structure. At the same time, we divided the spherical pores with a diameter of 0-600 μm in the bed into 12 parts at intervals of 50 μm. We counted the total pore volume in different diameter ranges. The changes in pore volume in different ranges at different bed heights with or without shear were plotted, as shown in Fig. 10. We can see that the pore volume in the range of 50-250 μm in diameter is the largest at different bed heights with and without shear, which is the main storage space for water in the thickening bed. In addition, as the bed height decreases without shear, the pore volume above 150 μm in diameter decreases to different degrees, and the pore volume below 150 μm in diameter increases slightly.

The data show that pore structures with diameters above 150 μm during bed drainage without shear are preferentially damaged and transformed into pores below 150 μm (Chen et al., 2023a). The pore volume in the 50-600 μm range in diameter decreased to different degrees as the bed height decreased with the shear condition. The data indicate that the pore structures in the bed with diameters in the range of 50-600 μm are damaged with rake shear. A comparison of the pore structure volumes with and without shear revealed that the reduction of pore volume in the bed with shear was more significant. The result is that the shear process changes the azimuthal angle of the coarse particles, creating a squeezing effect on the pore structure and promoting water discharge in the bed. Please refer to our previous study for this section (Li et al., 2023a).

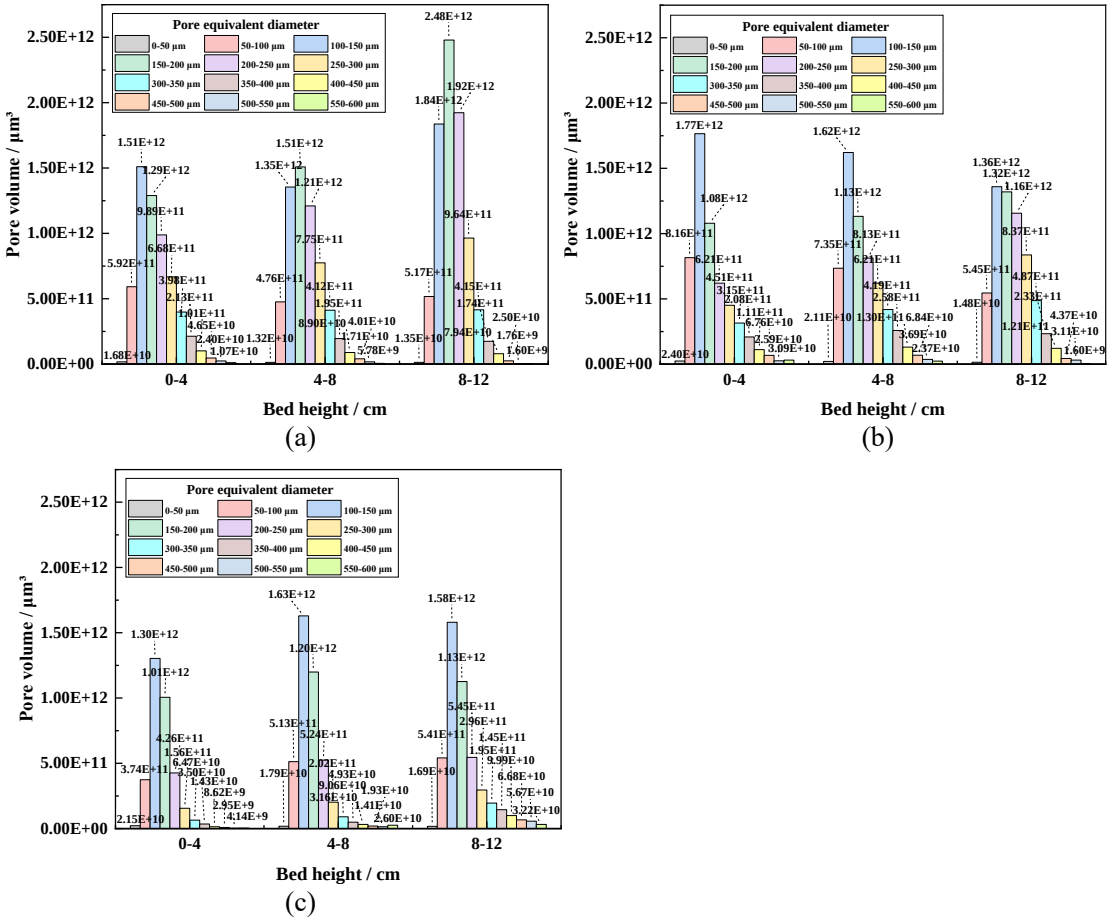

Fig. 10. The variation in pore volume with bed height in different diameter ranges in the bed: (a) 0 rpm-1 h, (b) 0 rpm-2 h, (c) 1 rpm-1 h.

Fig. 11 shows the variation in the proportion of isolated pore volume, spherical pore volume, and stick throat channel volume in the PNM with pore diameter for different ranges of equivalent diameters in the bed. We can see that the proportion of isolated pore volume in the bed decreases, and the proportion of spherical pore volume in the PNM increases as the equivalent diameter increases with and without shear. The proportion of stick throat volume in PNM decreases with the increase in equivalent diameter without shear. Meanwhile, the proportion of stick throat channel volume in PNM shows an increasing and then decreasing trend with the increase in equivalent diameter with shear. The main reason is that the shear effect of the rake increases the volume of isolated pores with equivalent diameters in the range of 0-50 μm.

In addition, we found that the pore volume in the range of 50-250 μm in pore diameter has a higher percentage of stick throat channel volume, as shown in the red area in Fig. 11. The data suggest that the stick throat channel structure in the range of 50-250 μm in pore diameter in the PNM is the main water storage space in the bed compared to the isolated pore structure in the bed and the spherical pore structure in the PNM (Chen et al., 2024; Chen et al., 2023a; Jiao et al., 2021).

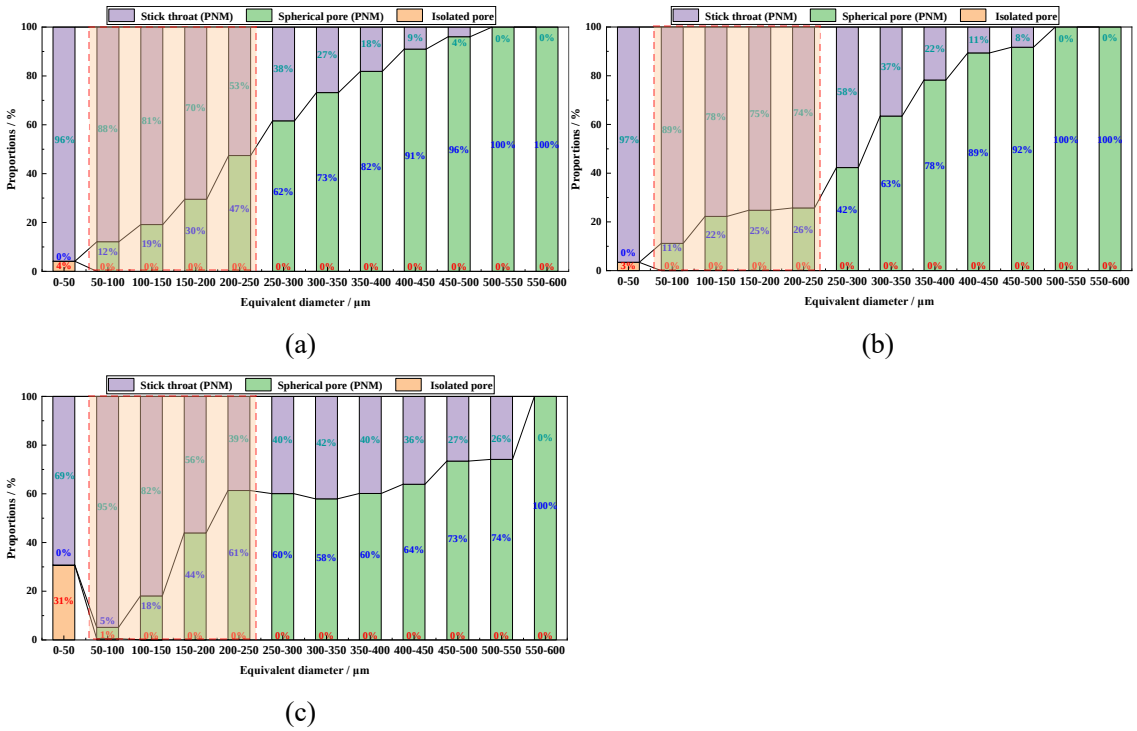

Fig. 11. The ratio of isolated pore volume, spherical pore volume, and stick throat channel volume varies with the equivalent diameter: (a) 0 rpm-1 h, (b) 0 rpm-2 h, (c) 1 rpm-1 h.

4.3 Difference in static yield stress between thickened tailings and fresh mixing slurry

Fig. 12 (a) and Fig. 12 (b) show the static yield stress of the thickened tailings in the thickening and the static yield stress of the fresh mixing slurry with the change of the slurry concentration, respectively. We found that the static yield stress of the thickening slurry is much larger than that of the fresh mixing slurry under the same slurry concentration and tailings gradation. The result suggests that when obtaining the rheological parameters of the slurry in the thickening bed, the structural state of the slurry should be consistent with the structural state of the slurry in the vertical sand silo or thickener. In other words, when measuring the rheological parameters of the slurry in the tailings thickening process, the slurry in the vertical sand silo or thickener should be sampled and measured in situ. Suppose the rheological measurement is carried out by using fresh mixing slurry. In that case, it will lead to severe errors in the data, leading to misjudgment of the slurry flowability in the vertical sand silo or thickener. The result will lead to production accidents such as slurry hardening in the vertical sand silo or thickener rake blockage, affecting mine safety production and personal safety.

We also found that the static yield stress of the thickened tailings and fresh mixing slurry increased with increasing slurry concentration, consistent with previous research findings (Li et al., 2023b; Zhu et al., 2023). Combined this with the data of section 3.1, we found that the static yield stress of the slurry decreases with the decrease of the bed height in the vertical sand silo or thickener, which indicates that the slurry at the bottom of the vertical sand silo or thickener has worse flowability and is more prone to hardening.

In addition, the static yield stress of the slurry with a residence time of 2 h was higher than that of the slurry with a residence time of 1 h without shear. The result indicates that the slurry concentration is improved with increased slurry residence time in the thickening equipment. However, the flowability of the slurry is reduced, which also increases the probability of slurry hardening. We compared the static yield stress of the slurry with and without shear conditions and found that the static yield stress of the slurry was higher with low-speed rake shear. The result also indicates that it is more difficult for flow to occur in the thickener and that the rake has to overcome more resistance during the shearing process.

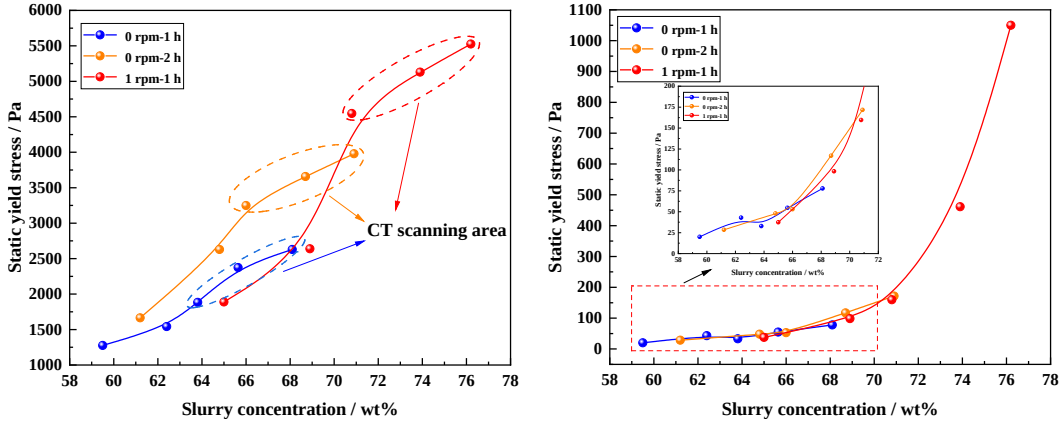

Fig. 12. Variation in static yield stress of slurry with slurry concentration: (a) thickened tailings, (b) fresh mixing slurry.

4.4 Variation in static yield stress of slurry with fine structural parameters

The flocculant solution flocculates with the tailings particle in the thickening process to form a floc structure. It settles to the bottom of the thickening equipment, and the floc structures are connected to form a thickened bed structure (Chen et al., 2023b; Zhu et al., 2023). The microscopic structures of the thickening bed at different heights are shown in Fig. 13(a). We can see apparent drainage channel structures of various sizes in the bed, indicating that the drainage channel structures in the thickening bed have strong anisotropy. Compared to the drainage channel structure in the bed with and without shear, we found that the number and size of the large drainage channel structures in the bed without shear were significantly larger than those with shear. The result indicated that the anisotropy of the drainage channel structures in the bed without shear was more substantial. The drainage channel structure with the rake shear is small, and there is no apparent large drainage channel structure, indicating that the shear action of the rake is beneficial to reducing the anisotropy of the drainage channel structure.

We found that due to the randomness of floc structure settling and the settling behavior of coarse particles, the distribution of coarse particles and drainage channel structure on the XY plane in the bed is inhomogeneous, and the schematic diagram is shown in Fig. 13 (b). Some of the coarse particles in the bed form a plugging effect on the drainage channel structure. The plugged small drainage channel structure is transformed into a large drainage channel structure under the bed

pressure, and its size and quantity are random, which leads to the strong anisotropy of the drainage channel structure on the XY plane in the thickening bed. When the fresh mixing slurry is configured for rheological parameter measurements under high-speed stirring in the mixer, the shear force is greater than the gravity of the particles and the strength of the slurry structure. The coarse particles in the bed and the drainage channel structure are uniformly distributed in the slurry structure to form a highly homogeneous slurry (Li et al., 2023b). The schematic diagram of coarse particles and drainage channel structure in fresh mixing slurry is shown in Fig. 13 (c).

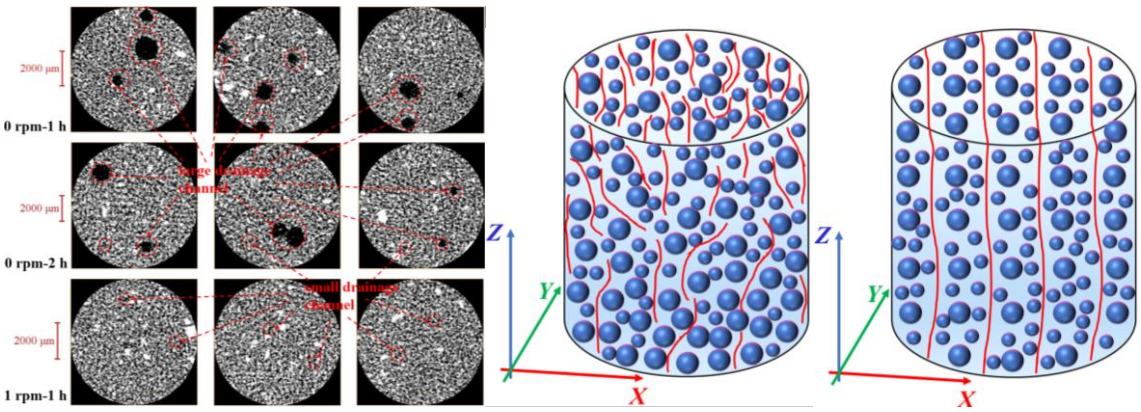

Fig. 13. Distribution of slurry structure: (a) Fine structure of thickening bed, (b) Schematic structure of thickened tailings, (c) Schematic structure of fresh mixing slurry.

We also found that the porosity of the thickening bed is closely related to the anisotropy of the drainage channel structure in the bed, and the stronger the anisotropy of the drainage channel structure, the greater the porosity fluctuation in the bed. Fig. 14 shows the variation in bed porosity at different bed heights with or without shear. We found that the porosity of the bed showed a fluctuating change with the decrease in the bed height, indicating that the thickened tailings belongs to the non-homogeneous slurry. Moreover, the fluctuation of bed porosity decreases with the increase of slurry residence time without shear. The result is that the large drainage channel structure is preferentially damaged during the drainage process and transformed into a small drainage channel structure. As the slurry residence time increases, the drainage channel volume in the bed gradually decreases, and the degree of transition from large to small drainage channel structures increases. The anisotropy between the drainage channel structures was gradually reduced, and the fluctuation of porosity was also steadily reduced. The coarse particles in the bed have a squeezing effect on the drainage channel structure with rake shear (Li et al., 2023a). It reduces the volume of the drainage channel and the anisotropy between the drainage channel structures at different bed heights, resulting in a significant reduction in the fluctuation of the bed porosity.

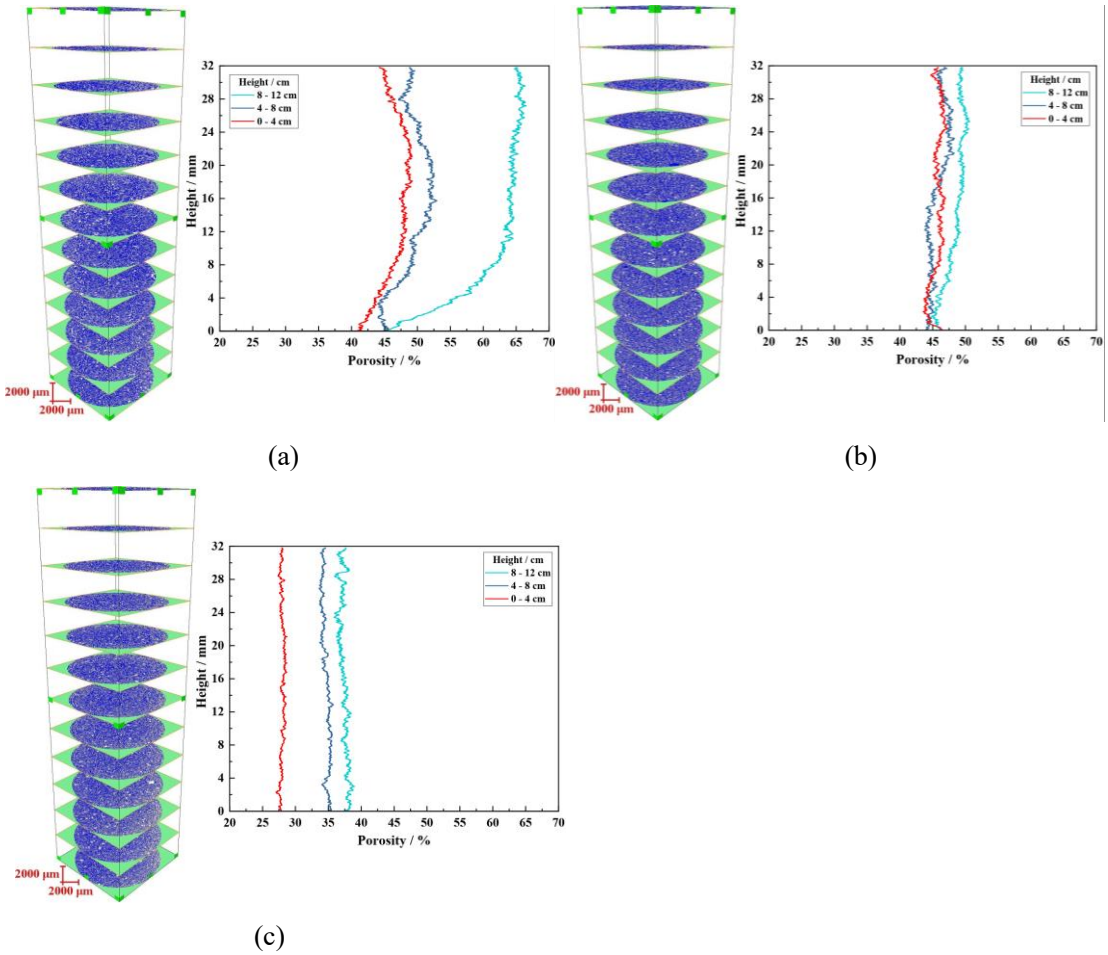

Fig. 14. Variation in 2D porosity with bed height in thickening beds: (a) 0 rpm-1 h, (b) 0 rpm-2 h, (c) 1 rpm-1 h.

Combined with the static yield stress measurements of the slurries in Section 4.1, we conclude that the fluctuation of the porosity of the thickening bed is responsible for the significant difference in static yield stress between the thickened tailings and the fresh mixing slurry under the same slurry concentration and particle gradation. To quantify the effect of the thickening bed porosity fluctuation on the slurry's static yield stress, we propose to use the coefficient of variation (*CV*) of bed porosity to characterize the fluctuation of the thickened tailings. The stronger the fluctuation of the porosity of the thickening bed, the larger the coefficient of variation in the bed porosity. The ratio of the static yield stress of the thickened tailings to the fresh mixing slurry at the same concentration and particle gradation is defined as T_{SYS}, as shown in Eq. 1. The coefficient of variation in bed porosity is calculated as shown in Eq. 2 (Brown, 1998).

$$T_{SYS} = SYS_{Settling} / SYS_{Fresh} \tag{1}$$

$$CV = S / \overline{X} \times 100\% = \sqrt{\frac{\sum_{i=1}^{n}\left(X - \overline{X}\right)^2}{n-1}} / \overline{X} \times 100\% \tag{2}$$

where $SYS_{Settling}$ is the static yield stress of the thickened tailings, Pa, SYS_{Fresh} is the static yield stress of the fresh mixing slurry, Pa, S is the standard deviation of bed porosity, %, $\overline{X}$ is the average value of bed porosity, %, X is the bed porosity, %, n is the number of bed CT images.

Fig. 15 shows the variation in T_{SYS} with the coefficient of variation in the porosity of the thickening bed. We find that when the coefficient of variation in bed porosity decreases from 792.1% to 103.6%, the T_{SYS} also decreases from 61.3 to 5.3. The data show that under the same conditions of slurry concentration and particle gradation, the greater the anisotropy of the pore structure of the thickening bed and the greater the fluctuation of the bed porosity, the more pronounced the enhancement of the static yield stress of thickened tailings is, and the more unlikely to be flowed by the slurry. We compared the coefficients of variation in bed porosity under the three experimental conditions and found that the coefficient of variation in thickening bed porosity decreases with decreasing bed height. The coefficient of variation in bed porosity decreases with increased slurry residence time without shear. The coefficient of variation in bed porosity decreases more obviously under the rake shear. The result also indicates that the fluctuation of thickened tailings porosity decreases with increasing slurry concentration.

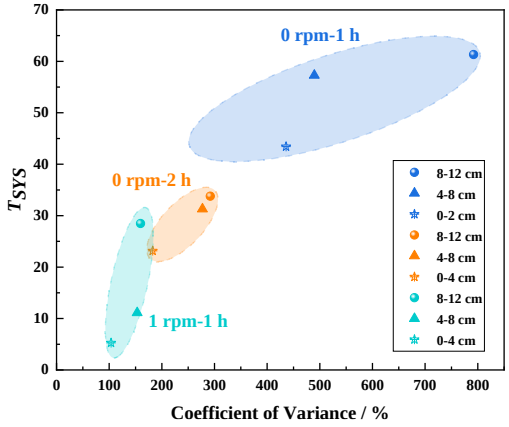

Fig. 15. Variation in T_{SYS} with bed porosity coefficient of variation.

5 Case study

The filling section of an iron ore mine in China uses a vertical sand silo for tailings thickening, which has a diameter of 8.8 m, a height of 24 m, and a storage capacity of 1,200 m³, as shown in Fig. 16 (a). The mine is filled with high-concentration slurry, and the underground mining void area is about 700,000 m³ per year. During the filling process of the mine, as the concentration of the thickened tailings increases, the thickened tailings is hardened at the bottom of the vertical sand silo, as shown in Fig. 16 (b). In the past, the mine used manual desludging to deal with the thickened tailings in the vertical sand silo. However, this method has a long working period and low efficiency, which not only consumes a lot of manpower and material resources but also adversely affects the normal filling production of the mine.

To ensure the filling body's strength and the filling economy, mines cannot reduce the concentration of the filling slurry and increase the cement-sand ratio. Based on the results of our study, the static yield stress of the thickened tailings can be substantially reduced, and the fluidity of the slurry can be improved by decreasing the anisotropy of the drainage channel structure of the thickening bed, i.e., by reducing the fluctuation of the porosity of the thickening thickened tailings.

For this purpose, we installed high-pressure air holes at the bottom of the vertical sand silo, as shown in Fig. 16 (c). The high-concentration thickened tailings at the bottom of the vertical sand silo is forced to shear by high-pressure gas, which reduces the fluctuation of the thickened tailings porosity and improves the flowability of the slurry at the bottom of the vertical sand silo, as shown in Fig. 16 (d). Based on the improved scheme, we reduced the static yield stress of the filling slurry from 1116.6 Pa to 89.3 Pa, improved the flowability of the slurry in the vertical sand silo without reducing the concentration of the filling slurry, solved the problem of slurry hardening in the vertical sand silo, and achieved safe, reliable and stable production.

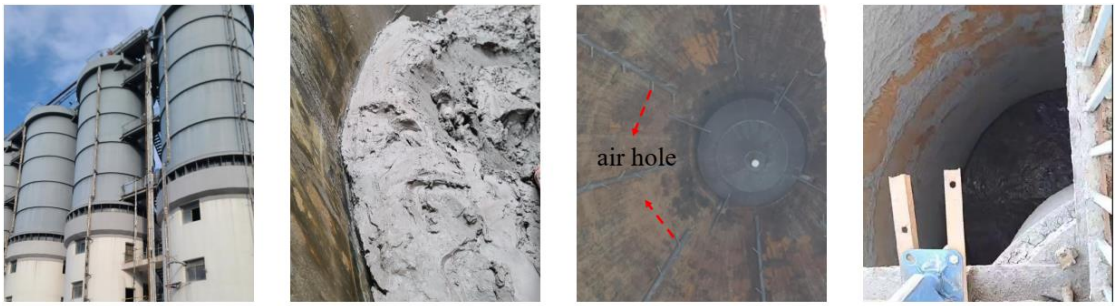

Fig. 16. Slurry consolidation in vertical sand silo and improvement effect: (a) Vertical sand silo, (b) Slurry hardening, (c) High-pressure air holes, (d) Slurry after forced shear.

6 Conclusion

(1) The concentration and static yield stress of the thickened tailings in both the vertical silo and the thickener increased with decreasing bed height. Both slurry residence time and rake shear increased the thickened tailings concentration and static yield stress. The static yield stress of the thickened tailings was much higher than that of the configured fresh mixing slurry for the same slurry concentration and particle gradation. The result suggests that in-situ sampling of the tailings thickened tailings formed by flocculation and settling should be used for rheological measurements to avoid obtaining erroneous data when obtaining the rheological parameters of the thickened tailings in the vertical sand silo and the thickener.

(2) Under the effect of bed pressure and rake shear, the compressive behavior of the bed structure occurs, the volume of coarse particles in the range of 75-300 μm in the bed increases, the volume of the drainage channel decreases, and the concentration of the slurry is improved. The PNM analysis indicated that the pore volume with the equivalent diameter in the 50-250 μm range was the largest, which was the main storage space for water in the bed. Stick throat channel volume proportion in the drainage channel structure decreases with the increase in the equivalent diameter. Compared with the spherical pore structure, the stick throat channel structure is the main component of the drainage channel structure in the bed.

(3) The anisotropy of the drainage channel structure in the thickening bed leads to fluctuation in the bed's porosity and increases the slurry's static yield stress. We propose to use the coefficient of variation in bed porosity to characterize the anisotropy of the slurry drainage channel structure of the

thickening bed. The results show that the greater the porosity fluctuation of the bed, the more pronounced the anisotropy of the drainage channel structure. The anisotropy of the drainage channel structure and the fluctuation of the slurry porosity decrease with the increase in the slurry concentration. Under the same slurry concentration and particle gradation, the stronger the fluctuation of the slurry porosity in the thickening bed, the greater the static yield stress of the slurry and the lower the slurry flowability. Based on the results of our research, it was applied in an iron ore mine in Anhui, China, where the flowability of the slurry in the vertical sand silo was improved by reducing the anisotropy of the porosity of the slurry in the thickening bed layer without decreasing the concentration of the filling slurry, solving the problem of slurry hardening in the vertical sand silo, and realizing a stable discharge of the bottom flow from the vertical sand silo. Therefore, this research provides ideas for solving the problems of slurry consolidation in the vertical sand silo bed and the thickener rake blockage problem.

It is worth noting that in this study, we assumed that the pore structure of the fresh slurry after mixing with a small high-speed mixer was homogeneous, and there was no apparent fluctuation in the porosity of the slurry at different bed heights, which is an assumption that has certain shortcomings. However, it is well known that the homogeneity of the tailings slurry after high-speed mixing has significantly improved, which is an indisputable fact. We also attempted to perform CT scanning on the stirred tailings slurry to obtain the microfine structure of the fresh mixing slurry. Unfortunately, the CT scan data of the fresh mixing slurry showed severe distortion and could not be analyzed effectively, as shown in Fig. 17. This result is that the structural strength of the fresh mixing slurry is lower than that of the thickening thickened tailings. During the CT scanning process, the coarse particles in the slurry and the bed structure undergo apparent settling behavior, which causes severe damage to the bed microstructure, thus making it impossible to obtain the microstructure of the fresh mixing slurry.

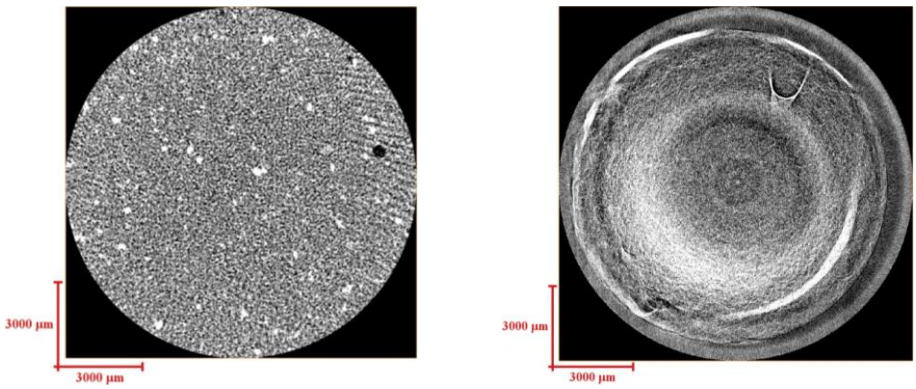

(a) (b)

Fig. 17. CT scan images of tailings slurry: (a) Thickened tailings, (b) Fresh mixing slurry.

CRediT authorship contribution statement

Gezhong Chen: Methodology, Investigation, Formal analysis, Software, Validation, Writing - original draft, Writing - review & editing. Cuiping Li: Conceptualization, Supervision, Methodology,

Funding acquisition, Writing - original draft, Writing - review & editing. Zhuen Ruan: Methodology, Investigation, Formal analysis, Software, Validation, Funding acquisition, Writing - review & editing. Raimund Bürger: Validation, Funding acquisition, Writing - review & editing. bingheng Yan: Methodology, Conceptualization, Software, Writing - review & editing. Chen Hu: Conceptualization, Software, Writing - review & editing. Xue Li: Methodology, Conceptualization, Software, Writing - review & editing.

Acknowledgements

This work was funded by the National Natural Science Foundation of China (52130404, 52304121), the National Key R&D Program of China (2022YFC2903803), the Fundamental Research Funds for the Central Universities (FRF-TP-22-112A1), Guangdong Basic and Applied Basic Research Foundation (no. 2021A1515110161), ANID (Chile) through Fondecyt project 1210610, Centro de Modelamiento Matemático (BASAL funds for Centers of Excellence FB210005), CRHIAM project ANID/FONDAP/15130015, and Anillo project ANID/ACT210030.

Conflict of Interest

All the authors declare that there is no conflict of interest regarding the publication of this paper.

References

Adiansyah, J.S., Rosano, M., Vink, S., Keir, G., 2015. A framework for a sustainable approach to mine tailings management: disposal strategies. J. Clean. Prod. 108, 1050–1062. https://doi.org/10.1016/j.jclepro.2015.07.139.

Adiguzel, D., Bascetin, A., 2019. The investigation of effect of particle size distribution on flow behavior of paste tailings. J. Environ. Manage. 243, 393–401. https://doi.org/10.1016/j.jenvman.2019.05.039.

Arjmand, R., Massinaei, M., Behnamfard, A., 2019. Improving flocculation and dewatering performance of iron tailings thickeners. J. Water Proc. Eng. 31, 100873. https://doi.org/10.1016/j.jwpe.2019.100873.

Asensi, E., Alemany, E., 2022. A hindered settling velocity model related to the fractal dimension and activated sludge flocs characteristics: Application to a sludge with a previous fragmentation and flocculation process. Sep. Purif. Technol. 300, 121812. https://doi.org/10.1016/j.seppur.2022.121812.

Boshrouyeh Ghandashtani, M., Costine, A., Edraki, M., Baumgartl, T., 2022. The impacts of high salinity and polymer properties on dewatering and structural characteristics of flocculated high-solids tailings. J. Clean. Prod. 342, 130726. https://doi.org/10.1016/j.jclepro.2022.130726.

Brown, C.E., 1998. Coefficient of Variation, in: Brown, C.E. (Ed.), Applied Multivariate Statistics in Geohydrology and Related Sciences. Springer, Berlin, Heidelberg, pp. 155–157. https://doi.org/10.1007/978-3-642-80328-4_13.

Carissimi, E., Rubio, J., 2015. Polymer-bridging flocculation performance using turbulent pipe flow. Miner. Eng. 70, 20–25. https://doi.org/10.1016/j.mineng.2014.08.019.

Chen, G., Li, C., Ruan, Z., Bürger, R., Gao, Y., Hou, H., 2023a. Structural evolution of bed drainage channels under the shear effect of the whole process of tailings thickening. Miner. Eng. 203, 108364. https://doi.org/10.1016/j.mineng.2023.108364.

Chen, G., Li, C., Ruan, Z., Bürger, R., Hou, H., 2024. A new permeability model of the compressible tailings thickening bed based on the throat structure parameters. Powder Technol. 433, 119263. https://doi.org/10.1016/j.powtec.2023.119263.

Chen, G., Li, C., Ruan, Z., Bürger, R., Hou, H., 2023b. Research on floc structure and physical properties based on pipeline flocculation. J. Water Proc. Eng. 53, 103627. https://doi.org/10.1016/j.jwpe.2023.103627.

Chen, Q., Zhou, H., Wang, Y., Wang, D., Zhang, Q., Liu, Y., 2023. Erosion wear at the bend of pipe during tailings slurry transportation: Numerical study considering inlet velocity, particle size and bend angle. Int. J. Miner. Metall. Mater. 30, 1608–1620. https://doi.org/10.1007/s12613-023-2672-z.

Fatt, I., 1956. The Network Model of Porous Media. Transactions of the AIME 207, 144–181. https://doi.org/10.2118/574-G.

Fawell, P.D., Nguyen, T.V., Solnordal, C.B., Stephens, D.W., 2021. Enhancing Gravity Thickener Feedwell Design and Operation for Optimal Flocculation through the Application of Computational Fluid Dynamics. Miner. Process. Extr. Metall. Rev. 42, 496–510. https://doi.org/10.1080/08827508.2019.1678156.

Gao, S., Li, W., Yuan, K., Rong, C., 2023. Properties and application of thixotropic cement paste backfill with molybdenum tailings. J. Clean. Prod. 391, 136169. https://doi.org/10.1016/j.jclepro.2023.136169.

Glotov, V.E., Chlachula, J., Glotova, L.P., Little, E., 2018. Causes and environmental impact of the gold-tailings dam failure at Karamken, the Russian Far East. Eng. Geol. 245, 236–247. https://doi.org/10.1016/j.enggeo.2018.08.012.

He, H., Liu, Y., Zhang, A., Yang, Z., Liu, X., Yang, R., Tang, H., Li, Z., 2023. Kinetic modeling and experimental verification of a swirl flocculation-enhanced reactor: A case study of coal chemical wastewater pretreatment. Sep. Purif. Technol. 326, 124852. https://doi.org/10.1016/j.seppur.2023.124852.

He, W., Chen, X., Xu, C., Zhou, C., Wang, C., 2023. Internal interaction between chemically-pretreated polypropylene microplastics and floc growth during flocculation: Critical effect on floc properties and flocculation mechanisms. Sep. Purif. Technol. 306, 122710. https://doi.org/10.1016/j.seppur.2022.122710.

Huazhe, J., Shufei, W., Yixuan, Y., Xinming, C., 2020. Water recovery improvement by shearing of gravity-thickened tailings for cemented paste backfill. J. Clean. Prod. 245, 118882. https://doi.org/10.1016/j.jclepro.2019.118882.

Jia, R., Zhang, B., He, D., Mao, Z., Chu, F., 2020. Data-driven-based self-healing control of abnormal feeding conditions in thickening–dewatering process. Miner. Eng. 146, 106141. https://doi.org/10.1016/j.mineng.2019.106141.

Jiao, H., Wu, Y., Wang, H., Chen, X., Li, Z., Wang, Y., Zhang, B., Liu, J., 2021. Micro-scale mechanism of sealed water seepage and thickening from tailings bed in rake shearing thickener. Miner. Eng. 173, 107043. https://doi.org/10.1016/j.mineng.2021.107043.

Langlois, J.I., Cipriano, A., 2019. Dynamic modeling and simulation of tailing thickener units for the development of control strategies. Miner. Eng. 131, 131–139. https://doi.org/10.1016/j.mineng.2018.11.006.

Lèbre, É., Corder, G.D., Golev, A., 2017. Sustainable practices in the management of mining waste: A focus on the mineral resource. Miner. Eng. 107, 34–42. https://doi.org/10.1016/j.mineng.2016.12.004.

Leite, A. da M.C., Reis, É.L., 2020. Cationic starches as flocculants of iron ore tailing slime. Miner. Eng. 148, 106195. https://doi.org/10.1016/j.mineng.2020.106195.

Li, C., Chen, G., Ruan, Z., Bürger, R., Gao, Y., Hou, H., Wang, H., 2023a. Effect of variations in the polar and azimuthal angles of coarse particles on the structure of drainage channels in thickened beds. Int. J. Miner. Metall. Mater. 30, 1–13. https://doi.org/10.1007/s12613-023-2680-z.

Li, C., Li, X., Ruan, Z., Huang, Z., Wang, H., 2023b. Analysis of homogeneity and rheological properties of filling slurry during the mixing process through electrical resistance tomography. Powder Technol. 428, 118850. https://doi.org/10.1016/j.powtec.2023.118850.

Li, X., Li, C., Ruan, Z., Yan, B., Hou, H., Chen, L., 2022. Analysis of particle migration and

agglomeration in paste mixing based on discrete element method. Constr. Build. Mater. 352, 129007. https://doi.org/10.1016/j.conbuildmat.2022.129007.
Lin, Z., Zhang, C., Hu, Y., Su, P., Quan, B., Li, X., Zhang, Z., 2023. Nano aluminum-based hybrid flocculant: Synthesis, characterization, application in mine drainage, flocculation mechanism. J. Clean. Prod. 399, 136582. https://doi.org/10.1016/j.jclepro.2023.136582.
Liu, Y., Zhang, X., Jiang, W., Wu, M., Li, Z., 2021. Comprehensive review of floc growth and structure using electrocoagulation: Characterization, measurement, and influencing factors. Chem. Eng. J. 417, 129310. https://doi.org/10.1016/j.cej.2021.129310.
MacIver, M.R., Pawlik, M., 2022. A floc structure perspective on sediment consolidation in thickened tailings. Chem. Eng. Sci. 263, 118095. https://doi.org/10.1016/j.ces.2022.118095.
Mashifana, T., Sithole, T., 2021. Clean production of sustainable backfill material from waste gold tailings and slag. J. Clean. Prod. 308, 127357. https://doi.org/10.1016/j.jclepro.2021.127357.
Murujew, O., Geoffroy, J., Fournie, E., Socionovo Gioacchini, E., Wilson, A., Vale, P., Jefferson, B., Pidou, M., 2020. The impact of polymer selection and dose on the incorporation of ballasting agents onto wastewater aggregates. Water Res. 170, 115346. https://doi.org/10.1016/j.watres.2019.115346.
O'Shea, J.-P., Qiao, G.G., Franks, G.V., 2010. Solid–liquid separations with a temperature-responsive polymeric flocculant: Effect of temperature and molecular weight on polymer adsorption and deposition. J. Colloid Interface Sci. 348, 9–23. https://doi.org/10.1016/j.jcis.2010.04.063.
Otus, N., 1979. A threshold selection method from gray-level histograms. a threshold selection method from gray-level histograms.
Peng, W., Lv, S., Cao, Y., Wang, W., Liu, S., Huang, Y., Fan, G., 2023. A novel pH-responsive flocculant for efficient separation and recovery of Cu and Mo from secondary resources via selective flocculation-flotation. J. Clean. Prod. 395, 136463. https://doi.org/10.1016/j.jclepro.2023.136463.
Qi, C., Fourie, A., 2019. Cemented paste backfill for mineral tailings management: Review and future perspectives. Miner. Eng. 144, 106025. https://doi.org/10.1016/j.mineng.2019.106025.
Qi, C., Fourie, A., Chen, Q., Tang, X., Zhang, Q., Gao, R., 2018. Data-driven modelling of the flocculation process on mineral processing tailings treatment. J. Clean. Prod. 196, 505–516. https://doi.org/10.1016/j.jclepro.2018.06.054.
Rana, N.M., Ghahramani, N., Evans, S.G., Small, A., Skermer, N., McDougall, S., Take, W.A., 2022. Global magnitude-frequency statistics of the failures and impacts of large water-retention dams and mine tailings impoundments. Earth-Sci. Rev. 232, 104144. https://doi.org/10.1016/j.earscirev.2022.104144.
Rico, M., Benito, G., Díez-Herrero, A., 2008. Floods from tailings dam failures. J. Hazard. Mater. 154, 79–87. https://doi.org/10.1016/j.jhazmat.2007.09.110.
Ruan, Z., Wu, A., Bürger, R., Betancourt, F., Wang, Yiming, Wang, Yong, Jiao, H., Wang, S., 2021. Effect of interparticle interactions on the yield stress of thickened flocculated copper mineral tailings slurry. Powder Technol. 392, 278–285. https://doi.org/10.1016/j.powtec.2021.07.008.
Sabah, E., Erkan, Z.E., 2006. Interaction mechanism of flocculants with coal waste slurry. Fuel 85, 350–359. https://doi.org/10.1016/j.fuel.2005.06.005.
Tan, C.K., Bao, J., Bickert, G., 2017. A study on model predictive control in paste thickeners with rake torque constraint. Miner. Eng. 105, 52–62. https://doi.org/10.1016/j.mineng.2017.01.011.
Trampus, B.C., França, S.C.A., 2020. Performances of two flocculants and their mixtures for red mud dewatering and disposal based on mineral paste production. J. Clean. Prod. 257, 120534. https://doi.org/10.1016/j.jclepro.2020.120534.
Walch, H., von der Kammer, F., Hofmann, T., 2022. Freshwater suspended particulate matter—Key components and processes in floc formation and dynamics. Water Res. 220, 118655.

https://doi.org/10.1016/j.watres.2022.118655.
Wang, C., Sun, C., Liu, Q., 2020. Formation, breakage, and re-growth of quartz flocs generated by non-ionic high molecular weight polyacrylamide. Miner. Eng. 157, 106546. https://doi.org/10.1016/j.mineng.2020.106546.
Wang, H., Wang, X., Wu, A., Peng, Q., 2021. A wall slip pressure gradient model of unclassified tailings paste in pipe flow: Theoretical and loop test study. J. Non-Newtonian Fluid Mech. 298, 104691. https://doi.org/10.1016/j.jnnfm.2021.104691.
Wu, A., Ruan, Z., Bürger, R., Yin, S., Wang, J., Wang, Y., 2020. Optimization of flocculation and settling parameters of tailings slurry by response surface methodology. Miner. Eng. 156, 106488. https://doi.org/10.1016/j.mineng.2020.106488.
Wu, A., Ruan, Z., Wang, J., 2022. Rheological behavior of paste in metal mines. Int. J. Miner. Metall. Mater. 29, 717–726. https://doi.org/10.1007/s12613-022-2423-6.
Xiong, Q., Baychev, T.G., Jivkov, A.P., 2016. Review of pore network modelling of porous media: Experimental characterisations, network constructions and applications to reactive transport. J. Contam. Hydrol. 192, 101–117. https://doi.org/10.1016/j.jconhyd.2016.07.002.
Ye, L., Wu, J., Huang, M., Yan, J., 2023. The role of suspended extracellular polymeric substance (EPS) on equilibrium flocculation of clay minerals in high salinity water. Water Res. 244, 120451. https://doi.org/10.1016/j.watres.2023.120451.
Yin, S., Shao, Y., Wu, A., Wang, H., Liu, X., Wang, Y., 2020. A systematic review of paste technology in metal mines for cleaner production in China. J. Clean. Prod. 247, 119590. https://doi.org/10.1016/j.jclepro.2019.119590.
Yu, W., Gregory, J., Campos, L., Li, G., 2011. The role of mixing conditions on floc growth, breakage and re-growth. Chem. Eng. J. 171, 425–430. https://doi.org/10.1016/j.cej.2011.03.098.
Zhang, L., Wang, H., Wu, A., Klein, B., Guo, J., Zhang, X., 2022. A zone settling velocity function to characterize settling properties of suspensions in thickening applications. Miner. Eng. 177, 107386. https://doi.org/10.1016/j.mineng.2021.107386.
Zhu, L., Lyu, W., Mao, X., Zhao, Z., Yang, D., Zhang, H., Wang, K., Yang, P., Zeng, H., 2023. Effect of solution pH and polyethylene oxide concentration on surface/interface properties, flocculation and rheology of concentrated monodisperse ultrafine synthetic tailings slurry. Powder Technol. 430, 119002. https://doi.org/10.1016/j.powtec.2023.119002.
Zhu, L., Lyu, W., Yang, P., Wang, Z., 2020. Effect of ultrasound on the flocculation-sedimentation and thickening of unclassified tailings. Ultrason. Sonochem. 66, 104984. https://doi.org/10.1016/j.ultsonch.2020.104984.